

[Article]

DOI: 10.13208/j.electrochem.201251

Http://electrochem.xmu.edu.cn

# Electrochemiluminescence Imaging Hydrogen Evolution Reaction on Single Platinum Nanoparticles Using a Bipolar Nanoelectrode Array

Xiang Qin, Zhong-Qiu Li, Jian-Bin Pan, Jian Li, Kang Wang, Xing-Hua Xia\*

(State Key Lab of Analytical Chemistry for Life Science, School of Chemistry and Chemical Engineering, Nanjing University, Nanjing 210023, Jiangsu China)

**Abstract:** A high-density ( $5.7 \times 10^8 \text{ cm}^{-2}$ ) nanoelectrode array with the electrode diameter of 200 nm and the interelectrode distance of 450 nm were fabricated. The nanoelectrode array consisted of gold nanowires embedded in a porous anodic aluminum oxide (AAO) matrix, having regular nanoelectrode distribution and highly uniform nanoelectrode size. The gold nanoelectrode array was used as a closed bipolar nanoelectrode array combined with electrochemiluminescence (ECL) method to map the electrocatalytic activity of platinum nanoparticles toward hydrogen evolution reaction (HER) by modifying the catalysts on single nanoelectrodes. Results show that HER on single bipolar nanoelectrodes could be imaged with the sub-micrometer spatial resolution. The present approach offers a platform to image local electrochemical activity of electrocatalytic materials, energy materials and cellular processes with high spatial resolution.

**Key words:** nanoelectrode array; bipolar electrode; electrochemiluminescence imaging; electrochemical imaging; single platinum nanoparticles; hydrogen evolution reaction

## 1 Introduction

Electrochemical analysis aims to qualitatively and quantitatively understand the evolution of electrochemically active species over time and space, and has been extensively used in a wide range of research fields including energy storage and conversion<sup>[1-4]</sup>, life science<sup>[5-7]</sup>, and electrocatalysis<sup>[8-10]</sup>. The local electrochemical information is of great importance to understand the processes occurring at molecular and/or atomic levels, for instances, it can provide valuable perspectives on micro-nano scaled objects, like single cells and nanostructured materials. In the past several decades, various electrochemical methods have been developed to obtain local electrochemical information. These techniques based on scanning probes, including scanning electrochemical microscopy (SECM)<sup>[10-12]</sup>, scanning ion conductance microscopy

(SICM)<sup>[13]</sup> and scanning electrochemical cell microscopy (SECCM)<sup>[1-3,9,14]</sup>, have encountered the same inevitable problem of limited scanning speed, and thus, time-consuming acquisition process. To overcome this issue, optics-related electrochemical methods have recently gained highly attraction, e.g., electrofluorochromism (EFC)<sup>[15-17]</sup> and electrochemiluminescence (ECL)<sup>[18-21]</sup> have been developed to image local electrochemical reactions. However, all these approaches are restricted in a particular class of reactions, namely, EFC reactions or ECL reactions, and powerless to map other redox reactions.

In order to extend the application fields of these optics-based electrochemical methods, Zhang's group has recently established a novel electrochemical imaging strategy through which a closed bipolar electrode array is introduced to couple an interested

**Citation:** Qin X, Li Z Q, Pan J B, Li J, Wang K, Xia X H. Electrochemiluminescence imaging hydrogen evolution reaction on single platinum nanoparticles using a bipolar nanoelectrode array. *J. Electrochem.*, 27(2): 157-167.

redox reaction with an EFC reaction<sup>[22]</sup> or an ECL reaction<sup>[23]</sup>, which converts electrochemical signals to optical ones that can be simply recorded by an EMCCD camera. Thus, any electrochemical process occurring at one side of the bipolar electrode array can be monitored through optical signals on the other side of the bipolar electrode array. However, the spatial resolution is limited by the micro scaled size of the individual carbon fibers (6  $\mu\text{m}$  in diameter) or carbon UMEs (8  $\mu\text{m}$  in diameter) in the arrays. Although gold wires (300  $\mu\text{m}$  in diameter) array embedded in an epoxy resin<sup>[24]</sup> and a gold electrode array (8  $\mu\text{m}$  in diameter) embedded in a track-etched membrane<sup>[25]</sup> have been used as closed bipolar electrode arrays for electrochemical imaging, the spatial resolution is yet constrained by large size of bipolar electrodes. These reports demonstrate that when nanoelectrode arrays are used, much improved spatial resolution for imaging can be achieved. Recently, we have fabricated high-density and superuniform nanoelectrode (60, 140, and 200 nm in diameter) arrays used for bipolar nanoelectrode arrays<sup>[26]</sup>. Coupled with an EFC reaction, a redox reaction on one side of the bipolar nanoelectrode array could be monitored by fluorescence on the other side. However, due to the rapid diffusion of fluorescence molecules, the spatial resolution for imaging was limited and the advantage of nanoelectrode array could not be exactly utilized.

Here, we fabricated highly uniform nanoelectrode arrays with very high nanoelectrode density of  $5.7 \times 10^8 \text{ cm}^{-2}$  as bipolar nanoelectrode arrays to map electrochemical heterogeneity. The nanoelectrode arrays are composed of gold nanowires embedded in anodic aluminum oxide (AAO) matrix with 200 nm of electrode diameter and 450 nm of interelectrode distance. Since ECL is a surface-confined process<sup>[19,20]</sup>, the ECL signal will be confined within the electrochemical active region of the nanoelectrode. We used this ECL reaction (Figure 1A) as the reporter to reflect the electrochemical reaction occurring on the other side of the bipolar nanoelectrode arrays, e.g., the reduction reaction of the target occurring at the cathodic pole of the bipolar nanoelectrode array, Ru (bpy)<sub>3</sub><sup>2+</sup>/TPrA will be accordingly oxidized at the anodic pole to generate

ECL signals that can be recorded by an EMCCD camera. We then monitored hydrogen evolution reaction (HER) on single platinum nanoparticles to demonstrate the high spatial resolution of the present electrochemical imaging platform.

## 2 Experimental Section

### 2.1 Chemicals and Materials

Porous anodic aluminum oxide (AAO) was purchased from Shenzhen TopMembranes Inc. (Shenzhen, China). Hydrogen tetrachloroaurate (III) trihydrate ( $\text{HAuCl}_4 \cdot 3\text{H}_2\text{O}$ ) was purchased from Alfa Aesar. Sodium sulfite ( $\text{Na}_2\text{SO}_3$ ), triammonium citrate, ethylenediamine tetraacetic acid (EDTA), potassium ferricyanide ( $\text{K}_3\text{Fe}(\text{CN})_6$ ), potassium ferrocyanide trihydrate ( $\text{K}_4\text{Fe}(\text{CN})_6 \cdot 3\text{H}_2\text{O}$ ), potassium dihydrogen phosphate ( $\text{KH}_2\text{PO}_4$ ) and dipotassium hydrogen phosphate trihydrate ( $\text{K}_2\text{HPO}_4 \cdot 3\text{H}_2\text{O}$ ) were obtained from Sino-pharm Chemical Reagent Co., Ltd. Sodium borohydride ( $\text{NaBH}_4$ ) and cysteamine hydrochloride were purchased from Shanghai Aladdin Biochemical Technology Co., Ltd. Hexaammineruthenium (III) chloride ( $\text{Ru}(\text{NH}_3)_6\text{Cl}_3$ ), tris(2,2'-bipyridyl)dichlororuthenium(II) hexahydrate ( $\text{Ru}(\text{bpy})_3\text{Cl}_2 \cdot 6\text{H}_2\text{O}$ ), chloroplatinic acid hexahydrate ( $\text{H}_2\text{PtCl}_6 \cdot 6\text{H}_2\text{O}$ ), sodium citrate, citric acid, L-ascorbic acid, tripropylamine (TPrA) and resazurin sodium salt were purchased from Sigma-Aldrich. All reagents were used as received without further purification. Milli-Q system purified water was used throughout all experiments.

### 2.2 Fabrications of Bipolar Nanoelectrode Arrays

A template-based electrodeposition method<sup>[26,27]</sup> was employed to prepare bipolar nanoelectrode arrays. The experimental details are demonstrated in the Supporting Information (Figure S1). Briefly, a silver layer ( $\sim 1 \mu\text{m}$ ) was coated on one side of porous anodic aluminum oxide (AAO) template by E-beam evaporation (Kurt J. Lesker, USA), serving as the working electrode for the electrodeposition process. A platinum disk and Hg/Hg<sub>2</sub>SO<sub>4</sub> electrode acted as the counter and the reference electrodes, respectively. The electrolyte containing 25  $\text{g} \cdot \text{L}^{-1}$  gold, 150  $\text{g} \cdot \text{L}^{-1}$  Na<sub>2</sub>SO<sub>3</sub>, 80  $\text{g} \cdot \text{L}^{-1}$  triammonium citrate and 60  $\text{g} \cdot \text{L}^{-1}$  EDTA in aqueous solution was adjusted to pH =  $\sim 7$ .

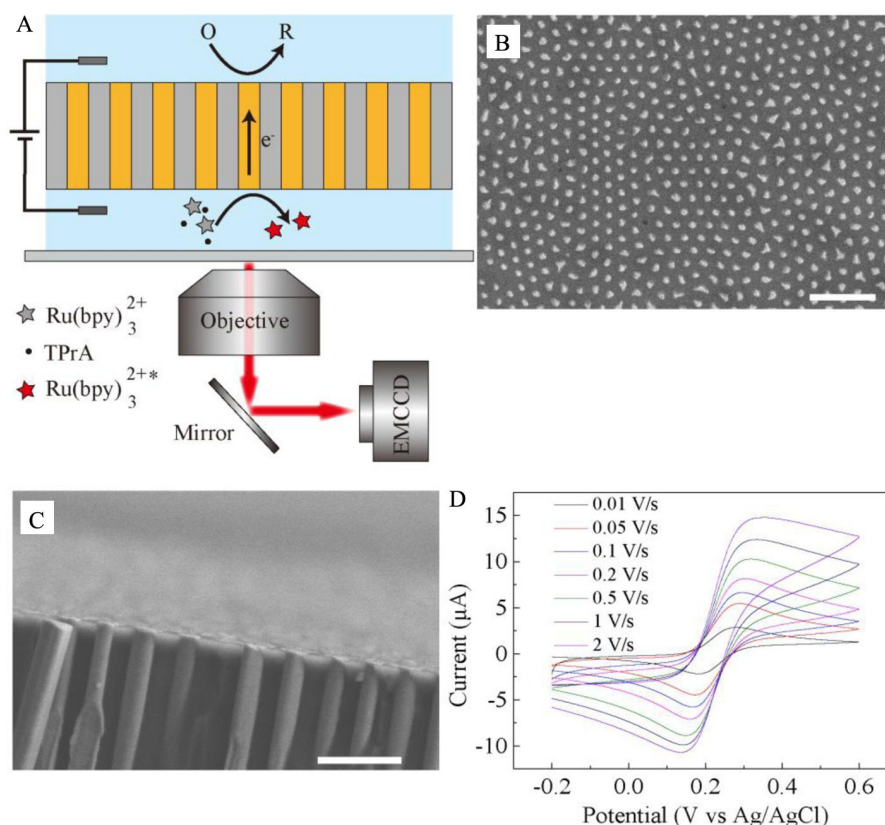


**Figure 1** (A) Schematic illustrating the principle of electrochemical imaging. (B) Top view SEM image of the nanoelectrode array with 200 nm diameter and 450 nm pitch. The scale bar is 2  $\mu\text{m}$ . (C) Cross-section SEM image of the nanoelectrode array. The scale bar is 1  $\mu\text{m}$ . (D) Voltammetric responses of the array at different scan rates. The electrolyte contained 1  $\text{mmol}\cdot\text{L}^{-1}$   $\text{K}_4\text{Fe}(\text{CN})_6$  and 0.1  $\text{mol}\cdot\text{L}^{-1}$  NaCl. (color on line)

Then, a pulse electrodeposition method (CHI 1140, CH Instruments) with 50  $\text{mA}\cdot\text{cm}^{-2}$  for 0.02 s and 0  $\text{mA}\cdot\text{cm}^{-2}$  for 0.98 s was used to perform the gold deposition process. In order to ensure that most pores of the AAO template were fully filled with gold, the gold nanowires were overgrown until a layer of Au was formed on the top of AAO membrane. Finally, the silver layer was dissolved with  $\text{HNO}_3$ . The overgrown gold film was polished with 3  $\mu\text{m}$ , 0.5  $\mu\text{m}$  diamond grinding discs, and 0.05  $\mu\text{m}$  diamond suspension (Buehler, USA) successively. Then, the AAO membrane was thoroughly washed with water and stored in pure ethanol for use as a bipolar nanoelectrode array.

### 2.3 Patterning the Bipolar Nanoelectrode Arrays and Pt Deposition

The bipolar nanoelectrode array was patterned with photoresist as a model to demonstrate the capa-

bility of electrochemical imaging. Arrays were spin coated with a thin layer of AZ 5214 photoresist (AZ Corporation) and prebaked at 85  $^{\circ}\text{C}$  for 90 s, followed by exposing the samples with a customized mask and a MA6-SCIL lithography system (SUSS, Germany). Then, the reversal baking was performed at 95  $^{\circ}\text{C}$  for 120 s to get a negative pattern of the mask. Patterning was accomplished by developing the sample in AZ developer solution, yielding a pattern with selectively exposed gold nanoelectrodes. Platinum ( $\sim 50$  nm) was deposited on the exposed gold nanoelectrodes using E-beam evaporation (Kurt J. Lesker, USA). The photoresist layer was removed by immersing the samples in N-Methyl pyrrolidone, which gave rise to selectively deposited platinum on partial gold nanoelectrodes, and the others remained exposed.

### 2.4 ECL Measurements and Imaging

A sample cell for bipolar ECL measurements and

imaging was designed as shown in Supporting Information (Figure S2). Bipolar voltage was applied using an electrochemical workstation (CHI 660E, CH Instruments) with two Ag/AgCl quasi-reference electrodes. ECL measurements were performed using a photomultiplier instrument (Remex Electronics Co. Ltd., China). A Nikon Eclipse Ti inverted microscope equipped with a  $60\times$  oil immersion objective (Nikon, Japan) and an electron multiplying charge coupled device (EMCCD, Princeton Instruments, USA) were used for ECL imaging. The exposure time for each image acquisition was 200 ms. A scan rate of  $0.2\text{ V}\cdot\text{s}^{-1}$  was used throughout the experiments. A home-made electronic device was used to synchronize the signals of EMCCD and electrochemical workstation.

For ECL imaging at single bipolar nanoelectrodes, the nanoelectrode array was modified with cysteamine to immobilize platinum nanoparticles. After assembling the sample cell, platinum nanoparticles solution was injected into the cathodic pole of the bipolar electrode. The imaging system was assembled with a Nikon Eclipse Ci upright microscope, a  $60\times$  water immersion objective (NA 1.0, Nikon, Japan) and an EMCCD with 1000 ms exposure time. A 2.4 V constant potential was applied across the bipolar electrodes to drive ECL at single nanoelectrodes.

### 3 Results and Discussion

#### 3.1 Fabrication and Characterization of Bipolar Nanoelectrode Arrays

It is noticeable that there are three main factors restricting the spatial resolution of our system: diameter and pitch of nanoelectrodes, diffusion of luminescent molecules and resolution of optical detection. In order to obtain electrochemical imaging with high spatial resolution, we first fabricated high-density nanoelectrode arrays by a template-based electrodeposition process. Porous anodic aluminum oxide (AAO) membrane with 200 nm pore diameter and 450 nm pore pitch was used as the template to fabricate bipolar nanoelectrode arrays, which yielded nanoelectrode arrays with 200 nm electrode diameter and 450 nm electrode pitch. Combined with a mechanical

polishing process after electrodeposition<sup>[26]</sup>, we fabricated the nanoelectrode array embedded in the AAO matrix with extremely flat surface. Figures 1(B) and (C) show the top view and the cross-section SEM images of the nanoelectrode array, respectively. It can be seen that almost all the pores of AAO membrane were completely filled with gold nanowires. Each gold nanowire embedded in the AAO membrane would serve as an independent closed bipolar nanoelectrode in the next electrochemical imaging experiments.

The electrochemical response of the gold nanoelectrode array was examined by cyclic voltammetry (CV). A gold layer was deposited on one side of the nanoelectrode array, serving as the working electrode. Figure 1D depicts the CVs of the nanoelectrode array in a solution of  $0.1\text{ mol}\cdot\text{L}^{-1}$  NaCl containing  $1\text{ mmol}\cdot\text{L}^{-1}$   $\text{K}_4\text{Fe}(\text{CN})_6$  at scan rates ranging from 0.01 to  $2\text{ V}\cdot\text{s}^{-1}$ . As expected, owing to the high density of the nanoelectrode array, the CVs display peak-shaped characteristics at all scan rates, which indicates total overlap of the diffusion layers of adjacent nanoelectrodes<sup>[28]</sup>. This result also demonstrates that the nanoelectrodes in the array are electrochemically active and very suitable for electrochemical imaging on account of high density.

#### 3.2 ECL on a Bipolar Nanoelectrode Array

To investigate the feasibility of the conversion from electrochemical signals to optical signals by a bipolar nanoelectrode array, we first utilized the nanoelectrode array to demonstrate the electrochemical coupling between the reduction of several model targets and the oxidation of  $\text{Ru}(\text{bpy})_3^{2+}/\text{TPrA}$ . The cathodic pole was placed in an aqueous solution of  $5\text{ mmol}\cdot\text{L}^{-1}$   $\text{Fe}(\text{CN})_6^{3-}$ ,  $5\text{ mmol}\cdot\text{L}^{-1}$   $\text{Ru}(\text{NH}_3)_6^{3+}$  or  $100\text{ mmol}\cdot\text{L}^{-1}$  phosphate buffer (pH = 7.4), while the ECL solution of  $100\text{ mmol}\cdot\text{L}^{-1}$  phosphate buffer (pH = 7.5) containing  $1\text{ mmol}\cdot\text{L}^{-1}$   $\text{Ru}(\text{bpy})_3^{2+}$  and  $50\text{ mmol}\cdot\text{L}^{-1}$  TPrA was injected into the anodic pole. A cyclic driving voltage was applied on the bipolar cell to reduce the targets and oxidize the  $\text{Ru}(\text{bpy})_3^{2+}/\text{TPrA}$  couple to generate ECL. In the previous studies<sup>[29-32]</sup>, the ECL intensity of  $\text{Ru}(\text{bpy})_3^{2+}/\text{TPrA}$  system on gold

electrodes dramatically decayed with the increase of potential cycles, particularly on gold nanoelectrodes, owing to the anodic dissolution of gold in the ECL solution containing chloride ions from  $\text{Ru}(\text{bpy})_3\text{Cl}_2$  and the formation of surface oxides on gold nanoelectrodes. Hence, we removed chloride ions from the ECL solution to circumvent the etching of gold and a nonionic fluorosurfactant, Zonyl FSN-100<sup>[33]</sup>, was used to modify the gold nanoelectrodes. The adsorbed surfactant layer renders the gold nanoelectrodes more hydrophobic and the access of  $\text{H}_2\text{O}$  molecules to the electrode surfaces can be precluded, therefore the formation of surface oxide is inhibited and the oxidation of TPrA will be facilitated, resulting in significant enhancement of the ECL intensity.

In order to obtain stable and strong ECL signals, the upper-limit potential of cyclic driving voltage was optimized. For the reduction of  $\text{Fe}(\text{CN})_6^{3-}$ , the optimal upper-limit potential is 1.2 V, at which the ECL signals show excellent stability and high intensity (Figure S3). Besides, the optimal upper-limit potentials are 1.7 V and 2.3 V for the reduction of  $\text{Ru}(\text{NH}_3)_6^{3+}$  and water, respectively. Figure 2A shows the ECL intensity-potential curves of three different targets. Strong ECL signals were observed when the driving voltages were greater than 0.8 V, 1.2 V and 1.6 V for  $\text{Fe}(\text{CN})_6^{3-}$ ,  $\text{Ru}(\text{NH}_3)_6^{3+}$  and water, respectively. Figure 2B further shows the ECL responses with different

concentrations of  $\text{Fe}(\text{CN})_6^{3-}$ . The ECL intensity increased with the increase of  $\text{Fe}(\text{CN})_6^{3-}$  concentration, showing a direct linear correlation of the increased ECL intensity with the concentration of  $\text{Fe}(\text{CN})_6^{3-}$  (Figure 2B, the inset).

### 3.3 Electrochemical Imaging Using a Bipolar Nanoelectrode Array

In order to demonstrate the function of electrochemical imaging using the bipolar nanoelectrode array, the nanoelectrode array was patterned with a layer of photoresist on the cathodic side only. As shown by the SEM image in Figure 3A, only the nanoelectrodes within the pattern were exposed to solution, while the remaining nanoelectrodes were blocked by photoresist without contact with the solution. The cathodic side patterned with photoresist was placed in  $100 \mu\text{mol}\cdot\text{L}^{-1} \text{K}_3\text{Fe}(\text{CN})_6$  and the other side was placed in the ECL solution of  $100 \text{mmol}\cdot\text{L}^{-1}$  PBS (pH = 7.5) containing  $1 \text{mmol}\cdot\text{L}^{-1} \text{Ru}(\text{bpy})_3^{2+}$ ,  $50 \text{mmol}\cdot\text{L}^{-1}$  TPrA, and 0.05% FSN. Figure 3B illustrates five snapshots at different potentials taken from a video recording throughout the potential sweep process. The ECL images captured at the anodic pole of the bipolar nanoelectrode array had the same shape with the pattern at the cathodic pole. The “NJU” pattern at the cathodic side can be imaged and well resolved at the anodic side of the bipolar nanoelectrode array. However, the pattern in the ECL images showed broadening

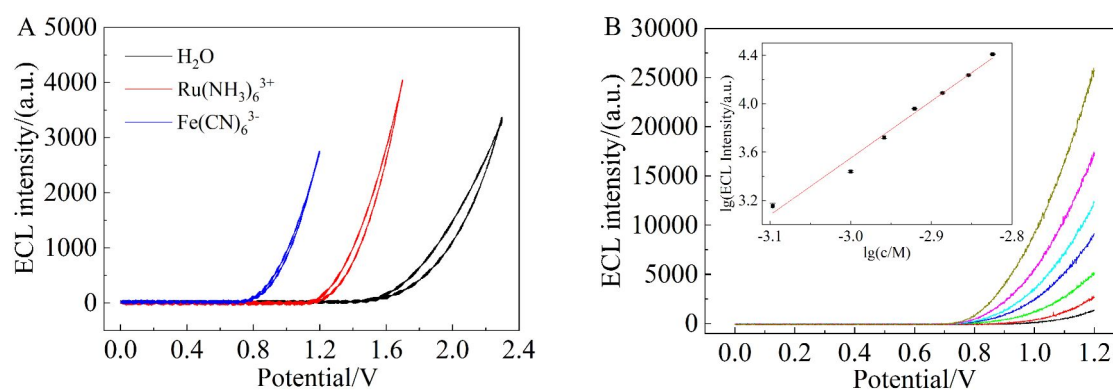


**Figure 2** (A) ECL intensity-potential curves of  $\text{Fe}(\text{CN})_6^{3-}$  (Blue),  $\text{Ru}(\text{NH}_3)_6^{3+}$  (red) and water (black) in the bipolar configuration, respectively. (B) ECL responses of  $\text{Fe}(\text{CN})_6^{3-}$  with different concentrations. The inset shows the linear relationship between the logarithm of ECL intensity and the logarithm of ferricyanide concentration. The ECL solution contained  $1 \text{mmol}\cdot\text{L}^{-1} \text{Ru}(\text{bpy})_3^{2+}$ ,  $50 \text{mmol}\cdot\text{L}^{-1}$  TPrA and  $100 \text{mmol}\cdot\text{L}^{-1}$  phosphate buffer (pH = 7.5) in the presence of 0.05% FSN. The scan rate was  $0.2 \text{V}\cdot\text{s}^{-1}$ . (color on line)

boundaries as compared to the photoetching pattern at the cathodic side, which is attributed to the diffusion of luminescent molecules. To roughly evaluate the influence of diffusion, strip-type patterns were prepared on the array and the corresponding ECL imaging was performed (Figure S4). The width of strips imaged by ECL was  $\sim 12.8 \mu\text{m}$ , which is much larger than the size of  $4.2 \mu\text{m}$  in the SEM image. This result implies that ECL molecules diffuse  $\sim 4.3 \mu\text{m}$  radially under the present experimental conditions, and thus, the spatial resolution is restricted to  $4.3 \mu\text{m}$  approximately. From the nanoelectrode array itself, the theoretical spatial resolution should be within 250 and 650 nm depending on the diameter and pitch of the nanoelectrodes. Thus, in our approach, the diffusion of luminescent molecules will lower the spatial resolution significantly. This can be completely prevented by immobilizing luminescent molecules on surface of the bipolar nanoelectrodes. Nevertheless, the quantity of immobilized molecules like monolayer modification is extremely limited and the detection limit will decrease remarkably. Thus, we propose to develop an effective method to immobilize luminescent molecules as many as possible onto the nanoelectrode surfaces. For demonstration, a fingerprint was created on a bipolar nanoelectrode array by finger touching and the secretions from the skin ridges of the fingerprint were transferred onto the array surface. The regions with the secretions blocked the electrochemical reaction of the redox molecules and the rest regions remained active (Figure S5(A)). The latent fingerprint was imaged in the ECL image as shown in Figure S5(B), ridges and furrows are clearly displayed. The recognition of latent fingerprints plays an indispensable role in criminal investigation work and personal identification. This powerful electrochemical imaging method shows promising for the recognition of latent fingerprints.

Besides ECL reaction that can be coupled with the redox reaction of interest by the bipolar nanoelectrode arrays, electrofluorochromic (EFC) reaction can also be used in the present experimental configuration. For comparison, resazurin which is highly fluorescent after reduction was used in the electro-

chemical imaging experiments. The same sample cell with the “NJU” pattern as used in the experiment of Figure 3 was employed to demonstrate the capability of the fluorescence coupled electrochemical imaging system. The ECL solution in the cathodic chamber was replaced by an EFC solution of  $100 \text{ mmol} \cdot \text{L}^{-1}$  PBS containing  $100 \mu\text{mol} \cdot \text{L}^{-1}$  resazurin. While  $100 \mu\text{mol} \cdot \text{L}^{-1}$   $\text{K}_3\text{Fe}(\text{CN})_6$  was replaced by  $100 \mu\text{mol} \cdot \text{L}^{-1}$   $\text{K}_4\text{Fe}(\text{CN})_6$  serving as the anodic solution. The fluorescence images (Figure S6) only show a gradually expanding light spot rather than a “NJU” pattern as demonstrated in the ECL images of Figure 3. Although a high frame rate of 33.9 fps was used, no spatial resolved “NJU” pattern could be captured in the fluorescence images. Compared with fluorescence excited by external light source, the ECL excited by electrical stimulation on electrode surface involves short-lifetime electrogenerated radicals, showing the surface-confined characteristics that provides much higher spatial resolution for imaging than fluorescence.

### 3.4 Electrochemical Imaging of HER on Platinum Film

A prominent merit of the present method is that one can map any important electrochemical reaction with high throughput and high spatial-temporal reso-

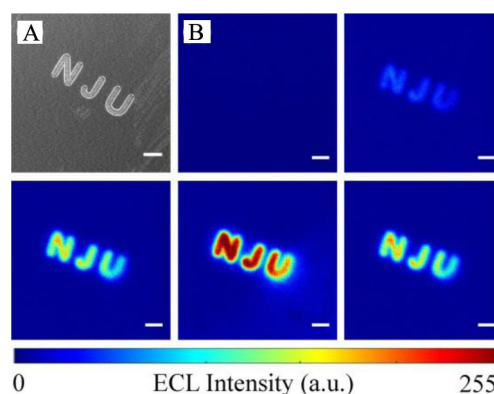


**Figure 3** (A) SEM image of the “NJU” pattern created by photoresist on one side of the array. (B) Five ECL snapshots recorded from a potential sweep experiment for detection of  $100 \mu\text{mol} \cdot \text{L}^{-1}$   $\text{Fe}(\text{CN})_6^{3-}$  in the cathodic pole using  $1 \text{ mmol} \cdot \text{L}^{-1}$   $\text{Ru}(\text{bpy})_3^{2+}$ ,  $50 \text{ mmol} \cdot \text{L}^{-1}$  TPrA and  $100 \text{ mmol} \cdot \text{L}^{-1}$  phosphate buffer (pH = 7.5) in the presence of 0.05% FSN in the anodic pole. Scale bars are  $20 \mu\text{m}$ .

lution. Hydrogen evolution reaction plays a key role in the production of renewable fuel<sup>[34, 35]</sup> and electrochemical imaging of HER is, thus, of great significance for developing efficient electrocatalysts. To demonstrate the electrochemical imaging of HER by the bipolar nanoelectrode array, a platinum pattern was created on one side of the nanoelectrode array, which was served as the electrocatalyst for water reduction. As shown in the first panel of Figure 4A, a “NJU” platinum film pattern with ~ 50 nm thickness was deposited on the gold nanoelectrode array. The patterned side of the bipolar nanoelectrode array was used as the cathodic pole and was placed in a solution of 100 mmol·L<sup>-1</sup> PBS (pH = 7.4). The anodic pole was filled with the same ECL solution as used above. As shown in Figure 4(A), during the potential scanning from 0 to 2.4 V, the increase of the cathodic current for HER was accompanied with the generation of more and more excited ruthenium molecules at the anode, which gives rise to the gradual enhancement of ECL intensity. The same “NJU” pattern as created on the cathodic side was well resolved in the ECL images at different potentials. The patterned platinum film showed higher HER activity than a bare gold nanoelectrode, as revealed by the appearance of the higher ECL intensity within the Pt film patterned regions. The variation of ECL intensity in two regions of interested (ROI) were analyzed, ROI-1 located at the region corresponding to the patterned platinum and ROI-2 located at the region corresponding to bare gold region as shown in the third panel of Figure 4(A). The resulting plots of the mean ECL intensity versus applied potential (Figure 4(C)) show that the ECL signals in ROI-1 emerge at lower potential and show the higher intensity than the signals in ROI-2.

In order to verify that the pattern indeed resulted from the electrocatalysis of platinum, water reduction reaction was replaced with the reduction of 5 mmol·L<sup>-1</sup> Ru(NH<sub>3</sub>)<sub>6</sub><sup>3+</sup> in 100 mmol·L<sup>-1</sup> PBS as a control. A voltage of 0 ~ 1.8 V was applied on the bipolar electrode array for the reduction of Ru(NH<sub>3</sub>)<sub>6</sub><sup>3+</sup>. Water was reduced by an inner-sphere mechanism, while Ru(NH<sub>3</sub>)<sub>6</sub><sup>3+</sup> was reduced by an outer-sphere mechanism. That

means that the electrode material has a profound effect on the electron transfer kinetics of water reduction reaction, while little effect on the reduction of Ru(NH<sub>3</sub>)<sub>6</sub><sup>3+</sup>. As seen in Figure 4(B), the whole array showed almost uniform ECL and the “NJU” pattern could not be visualized within the applied potential window. The variation of ECL intensity in the same regions of interest, ROI-1 and ROI-2, were also analyzed as shown in Figure 4D. The ECL signals in ROI-1 and ROI-2 appeared at the same potential and showed almost the same intensity. The voltammetric responses of a Pt disk electrode and an Au disk electrode in the same solutions of PBS or Ru(NH<sub>3</sub>)<sub>6</sub><sup>3+</sup> are shown in Figures S7(A) and (B), respectively. As expected the reduction of water was strongly dependent on the electrode material, while the reduction of Ru(NH<sub>3</sub>)<sub>6</sub><sup>3+</sup> not. For the reduction of water, the Pt electrode showed lower onset potential and greater current response than the gold electrode. The Pt electrode and gold electrode in Ru(NH<sub>3</sub>)<sub>6</sub><sup>3+</sup> responded almost the same.

### 3.5 Lighting up Single Bipolar Nanoelectrodes with Platinum Nanoparticles

As discussed above, although diffusion of luminescent molecules lowers the spatial resolution dramatically, it can be circumvented by activating sparsely distributed single bipolar nanoelectrodes, as a consequence, the influence of diffusion can be minimized. Scattered platinum nanoparticles with ca. 100 nm diameter (Figures S8 and S9) were modified on single gold nanoelectrodes by cysteamine as the linker and used to catalyze water reduction at single gold nanoelectrodes. As shown in Figure 5(A), those bipolar nanoelectrodes modified with platinum nanoparticles at the cathodic pole had higher electrocatalytic activity toward water reduction. Thus, at the anodic pole, they showed significantly higher ECL intensities than the bare gold bipolar nanoelectrodes. Figure 5(B) shows a representative ECL image of a single bipolar nanoelectrode. A typical 3D ECL intensity surface plot of a single bipolar nanoelectrode is displayed in Figure 5C. To ensure the signals indeed from platinum nanoparticles, the ECL images (Figure S10) before and

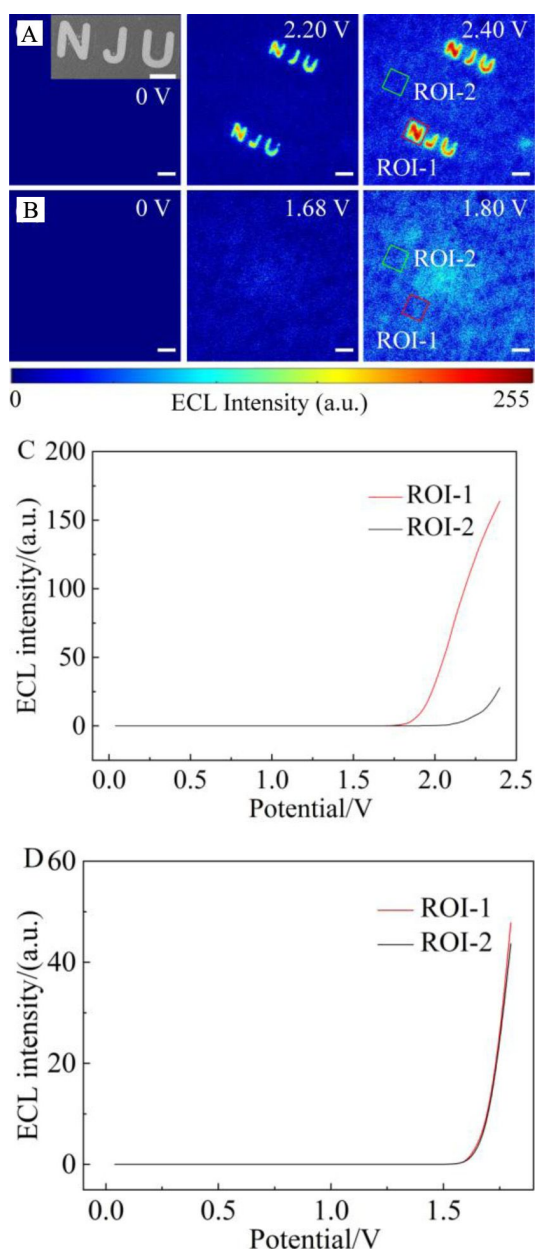


**Figure 4** A series of corresponding ECL images captured from a video recorded during the potential sweep experiment for the reductions of water (A) and Ru(NH<sub>3</sub>)<sub>6</sub><sup>3+</sup> (B). The inset in (A) shows the SEM image of patterned Pt film on the cathodic pole of the array. (C, D) ECL intensity-potential responses in Pt film region (ROI-1, red curve) and bare gold region (ROI-2, blue curve) extracted from the video recording of the reductions of water (C) and Ru(NH<sub>3</sub>)<sub>6</sub><sup>3+</sup> (D). All scale bars are 20  $\mu\text{m}$ .

after the injections of platinum nanoparticles were captured. Bright light spots appeared after the injection of platinum nanoparticles, which is the consequence of coupling between water reduction on plat-

inum nanoparticles and ECL of Ru(bpy)<sub>3</sub><sup>2+</sup> on anode. On account of diffraction limit, an optical microscopic system has a limited spatial resolution  $R = 0.61\lambda/\text{NA}$  ( $\lambda$  is the emission wavelength and NA is the numerical aperture of the objective). Hence, in spite of the effect of diffusion, the spatial resolution is estimated to be  $\sim 370$  nm under our experimental conditions. Figures 5(D) and 5(E) show the enlarged ECL images of three and two adjacent single nanoparticles, respectively. Since only three or two nanoelectrodes emitted light among lots of nanoelectrodes, diffusion of luminescent molecules had little influence on the spatial resolution. Thus, three or two adjacent single nanoparticles can be resolved as shown in Figures 5(D) and 5(E), and the sub-micrometer spatial resolution could be achieved. Nevertheless, in this way only a small part of nanoelectrodes was utilized. Solid-state ECL materials, such as quantum dots<sup>[36]</sup> and luminescent complex film<sup>[37]</sup>, might be used to eradicate the influence of diffusion, which is ongoing in our group.

## 4 Conclusions

The bipolar nanoelectrode arrays with high-density gold nanowires have been fabricated by electrodeposition of gold in AAO membranes. The gold nanowires in the arrays had extremely uniform length and the surfaces of the whole array were extremely flat. Different patterns were created on one side of the arrays and Ru(bpy)<sub>3</sub><sup>2+</sup>/TPPrA system was used as the luminescent reagents to demonstrate the capability of electrochemical imaging using the bipolar nanoelectrode array. In addition, the electrochemical imaging of hydrogen evolution reaction on platinum catalysts was performed, allowing monitoring electrocatalytic heterogeneity. Furthermore, the platinum nanoparticles were modified on the nanoelectrodes to light up single bipolar nanoelectrodes. Accordingly, the sub-micrometer spatial resolution could be achieved by performing electrochemiluminescence (ECL) imaging at single bipolar nanoelectrodes. The presently established electrochemical imaging platform possesses high spatial resolution. One can further improve the spatial resolution through adjusting the size

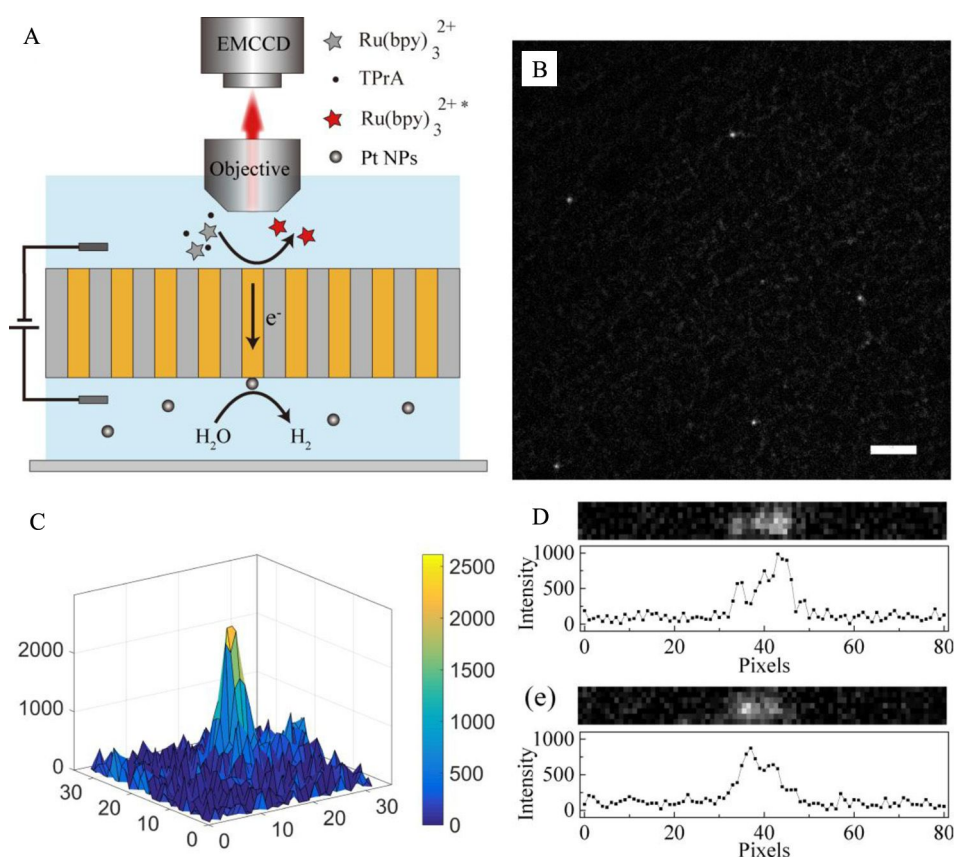


**Figure 5** (A) Schematic of ECL imaging on single bipolar nanoelectrodes. (B) A representative ECL image of single bipolar nanoelectrodes. The scale bar is 20  $\mu\text{m}$ . (C) A typical 32 $\times$ 32 pixels 3D ECL intensity surface plot of a single nanoelectrode. (D, E) ECL images of three (D) and two (E) adjacent nanoelectrodes and the corresponding intensity line profiles.

of the electrode arrays and by preventing the luminescent molecules from diffusion, which are being carried out in our group. We believe that this is an effective and universal approach for electrochemical imaging with high spatial-temporal resolution.

### Supporting Information

The Supporting Information is available free of charge on the website of *Journal of Electrochemistry*.

Schematic fabrication process of the nanoelectrode arrays, schematic of homemade sample cell, optimization of the ECL end potentials, the electrochemical imaging of the strip-type patterns, the electrochemical imaging of fingerprints, the electrochemical imaging of fluorescence coupling, HER on a platinum disk and a gold disk electrodes, synthesis of platinum nanoparticles, TEM image of platinum nanoparticles, SEM images of platinum nanoparticles on single bipolar nanoelectrodes, ECL images before

and after the injections of platinum nanoparticles.

### Acknowledgements

This work was supported by the National Key Research and Development Program of China (2017YFA0700500), the National Natural Science Foundation of China (No. 21635004, No. 21627806) and the Excellent Research Program of Nanjing University (No. ZYJH004).

### References:

- [1] Tao B L, Yule L C, Daviddi E, Bentley C L, Unwin P R. Correlative electrochemical microscopy of Li-ion (De)intercalation at a series of individual  $\text{LiMn}_2\text{O}_4$  particles[J]. *Angew. Chem. Int. Ed.*, 2019, 58(14): 4606-4611.
- [2] Sharel P E, Kang M, Wilson P, Meng L C, Perry D, Basile A, Unwin P R. High resolution visualization of the redox activity of  $\text{Li}_2\text{O}_2$  in non-aqueous media: conformal layer vs. toroid structure[J]. *Chem. Commun.*, 2018, 54(24): 3053-3056.

- [3] Takahashi Y, Kumatani A, Munakata H, Inomata H, Ito K, Ino K, Shiku H, Unwin P R, Korchev Y E, Kanamura K, Matsue T. Nanoscale visualization of redox activity at lithium-ion battery cathodes[J]. *Nat. Commun.*, 2014, 5: 5450.
- [4] Jiang D, Jiang Y Y, Li Z M, Liu T, Wo X, Fang Y M, Tao N J, Wang W, Chen H Y. Optical imaging of phase transition and Li-ion diffusion kinetics of single LiCoO<sub>2</sub> nanoparticles during electrochemical cycling[J]. *J. Am. Chem. Soc.*, 2016, 139(1): 186-192.
- [5] Bucher E S, Wightman R M. Electrochemical analysis of neurotransmitters[J]. *Annu. Rev. Anal. Chem.*, 2015, 8: 239-261.
- [6] Zhang J J, Zhou J Y, Pan R R, Jiang D C, Burgess J D, Chen H Y. New frontiers and challenges for single-cell electrochemical analysis[J]. *ACS. Sens.*, 2018, 3(2): 242-250.
- [7] Lin T E, Rapino S, Girault H H, Lesch A. Electrochemical imaging of cells and tissues[J]. *Chem. Sci.*, 2018, 9(20): 4546-4554.
- [8] Bentley C L, Kang M, Unwin P R. Nanoscale surface structure-activity in electrochemistry and electrocatalysis [J]. *J. Am. Chem. Soc.*, 2019, 141(6): 2179-2193.
- [9] Bentley C L, Kang M, Unwin P R. Nanoscale structure dynamics within electrocatalytic materials[J]. *J. Am. Chem. Soc.*, 2017, 139(46): 16813-16821.
- [10] Kim J, Renault C, Nioradze N, Arroyo-Curras N, Leonard K C, Bard A J. Electrocatalytic activity of individual Pt nanoparticles studied by nanoscale scanning electrochemical microscopy[J]. *J. Am. Chem. Soc.*, 2016, 138(27): 8560-8568.
- [11] Polcari D, Dauphin-Ducharme P, Mauzeroll J. Scanning electrochemical microscopy: A comprehensive review of experimental parameters from 1989 to 2015[J]. *Chem. Rev.*, 2016, 116(22): 13234-13278.
- [12] Kai T, Zoski C G, Bard A J. Scanning electrochemical microscopy at the nanometer level[J]. *Chem. Commun.*, 2018, 54(16): 1934-1947.
- [13] Kang M, Perry D, Bentley C L, West G, Page A, Unwin P R. Simultaneous topography and reaction flux mapping at and around electrocatalytic nanoparticles[J]. *ACS Nano*, 2017, 11(9): 9525-9535.
- [14] Daviddi E, Gonos K L, Colburn A W, Bentley C L, Unwin P R. Scanning electrochemical cell microscopy (SECCM) chronopotentiometry: Development and applications in electroanalysis and electrocatalysis[J]. *Anal. Chem.*, 2019, 91(14): 9229-9237.
- [15] Audebert P, Miomandre F. Electrofluorochromism: from molecular systems to set-up and display[J]. *Chem. Sci.*, 2013, 4(2): 575-584.
- [16] Sambur J B, Chen T Y, Choudhary E, Chen G, Nissen E J, Thomas E M, Zou N, Chen P. Sub-particle reaction and photocurrent mapping to optimize catalyst-modified photoanodes[J]. *Nature*, 2016, 530(7588): 77-80.
- [17] Bouffier L, Doneux T. Coupling electrochemistry with *in situ* fluorescence (confocal) microscopy[J]. *Curr. Opin. Electrochem.*, 2017, 6(1): 31-37.
- [18] Zhu M J, Pan J B, Wu Z Q, Gao X Y, Zhao W, Xia X H, Xu J J, Chen H Y. Electrogenerated chemiluminescence imaging of electrocatalysis at a single Au-Pt Janus nanoparticle[J]. *Angew. Chem. Int. Ed.*, 2018, 57(15): 4010-4014.
- [19] Valenti G, Scarabino S, Goudeau B, Lesch A, Jovic M, Villani E, Sentic M, Rapino S, Arbault S, Paolucci F, Sojic N. Single cell electrochemiluminescence imaging: from the proof-of-concept to disposable device-based analysis[J]. *J. Am. Chem. Soc.*, 2017, 139(46): 16830-16837.
- [20] Voci S, Goudeau B, Valenti G, Lesch A, Jovic M, Rapino S, Paolucci F, Arbault S, Sojic N. Surface-confined electrochemiluminescence microscopy of cell membranes[J]. *J. Am. Chem. Soc.*, 2018, 140(44): 14753-14760.
- [21] Zhou J Y, Ma G Z, Chen Y, Fang D J, Jiang D C, Chen H Y. Electrochemiluminescence imaging for parallel single-cell analysis of active membrane cholesterol[J]. *Anal. Chem.*, 2015, 87(16): 8138-8143.
- [22] Guerrette J P, Percival S J, Zhang B. Fluorescence coupling for direct imaging of electrocatalytic heterogeneity [J]. *J. Am. Chem. Soc.*, 2013, 135(2): 855-861.
- [23] Anderson T J, Defnet P A, Zhang B. Electrochemiluminescence (ECL) - based electrochemical imaging using a massive array of bipolar ultramicroelectrodes [J]. *Anal. Chem.*, 2020, 92(9): 6748-6755.
- [24] Iwama T, Inoue K Y, Abe H, Matsue T. Chemical imaging using a closed bipolar electrode array [J]. *Chem. Lett.*, 2018, 47(7): 843-845.
- [25] Iwama T, Inoue K Y, Abe H, Matsue T, Shiku H. Bioimaging using bipolar electrochemical microscopy with improved spatial resolution[J]. *Analyst*, 2020, 145(21): 6895-6900.
- [26] Qin X, Li Z Q, Zhou Y, Pan J B, Li J, Wang K, Xu J J, Xia X H. Fabrication of high-density and superuniform gold nanoelectrode arrays for electrochemical fluorescence imaging[J]. *Anal. Chem.*, 2020, 92(19): 13493-13499.
- [27] Hurst S J, Payne E K, Qin L, Mirkin C A. Multisegmental one-dimensional nanorods prepared by hard-template

- synthetic methods[J]. *Angew. Chem. Int. Ed.*, 2006, 45(17): 2672-2692.
- [28] Peinetti A S, Gilardoni R S, Mizrahi M, Requejo F G, Gonzalez G A, Battaglini F. Numerical simulation of the diffusion processes in nanoelectrode arrays using an axial neighbor symmetry approximation[J]. *Anal. Chem.*, 2016, 88(11): 5752-5759.
- [29] Zu Y, Bard A J. Electrogenenerated chemiluminescence. 66. The role of direct coreactant oxidation in the ruthenium Tris(2,2')bipyridyl/triethylamine system and the effect of halide ions on the emission intensity[J]. *Anal. Chem.*, 2000, 72(14): 3223-3232.
- [30] Pan S, Liu J, Hill C M. Observation of local redox events at individual Au nanoparticles using electrogenerated chemiluminescence microscopy[J]. *J. Phys. Chem. C*, 2015, 119(48): 27095-27103.
- [31] Wilson A J, Marchuk K, Willets K A. Imaging electro-generated chemiluminescence at single gold nanowire electrodes[J]. *Nano. Lett.*, 2015, 15(9): 6110-6115.
- [32] Valenti G, Fiorani A, Li H, Sojic N, Paolucci F. Essential role of electrode materials in electrochemiluminescence applications[J]. *ChemElectroChem*, 2016, 3(12): 1990-1997.
- [33] Li F, Zu Y. Effect of nonionic fluorosurfactant on the electrogenerated chemiluminescence of the tris(2,2'-bipyridine)ruthenium(II)/Tri-n-propylamine system: lower oxidation potential and higher emission intensity[J]. *Anal. Chem.*, 2004, 76(6): 1768-1772.
- [34] Yin H J, Zhao S L, Zhao K, Muqsit A, Tang H J, Chang L, Zhao H J, Gao Y, Tang Z Y. Ultrathin platinum nanowires grown on single-layered nickel hydroxide with high hydrogen evolution activity[J]. *Nat. Commun.*, 2015, 6: 6430.
- [35] Cheng N, Stambula S, Wang D, Banis M N, Liu J, Riese A, Xiao B, Li R, Sham T K, Liu L M, Botton G A, Sun X L. Platinum single-atom and cluster catalysis of the hydrogen evolution reaction[J]. *Nat. Commun.*, 2016, 7: 13638.
- [36] Liu S F, Zhang X, Yu Y M, Zou G Z. A monochromatic electrochemiluminescence sensing strategy for dopamine with dual-stabilizers-capped CdSe quantum dots as emitters[J]. *Anal. Chem.*, 2014, 86(5): 2784-2788.
- [37] Wei H, Wang E K. Solid-state electrochemiluminescence of tris(2,2'-bipyridyl) ruthenium [J]. *TRAC-Trend Anal. Chem.*, 2008, 27(5): 447-459.

## 双极纳米电极阵列实现单个铂纳米颗粒上 氢气析出反应的电致化学发光成像

秦 祥,李仲秋,潘建斌,李 剑,王 康,夏兴华\*

(生命分析化学国家重点实验室,南京大学化学化工学院,江苏 南京)

**摘要:** 本文制备了嵌于多孔阳极氧化铝(AAO)膜中直径为200 nm,间距为450 nm的高密度( $5.7 \times 10^8 \text{ cm}^{-2}$ )的金纳米电极阵列,纳米电极分布规则,尺寸高度均一。我们将该金纳米电极阵列作为双极电极阵列,可将电极一侧的电化学法拉第信号在另一侧电极上转化成电致化学发光(ECL)信号,从而实现单个铂纳米颗粒上氢气析出反应(HER)进行亚微米空间分辨率的电化学成像。本文介绍的方法为高空间分辨率成像电催化材料、能源材料以及细胞过程的局部电化学活性提供了一个良好的平台。

**关键词:** 纳米电极阵列;双极电极;电致化学发光成像;电化学成像;单个铂纳米颗粒;氢气析出反应